

Investigation of pinholes in Czochralski silicon ingots in relation to structure loss

Authors: Øyvind S. Sortland^{*,a}, Eivind J. Øvreid^{a,b}, Mohammed M'Hamdi^{a,b}, Marisa Di Sabatino^a

Affiliations:

^a NTNU, Department of Materials Science and Engineering, Trondheim, Norway

^b SINTEF Industry, Trondheim/Oslo, Norway

* Corresponding author. E-mail address: oyvind.sunde.sortland@ntnu.no

Declaration of interest: Øyvind S. Sortland is employed with leave of absence from the monocrystalline silicon ingot and wafer producer NorSun AS.

In the production of monocrystalline silicon by the Czochralski process, structure loss frequently reduces yield and increases production time. Structure loss means the transition from monocrystalline to multicrystalline structure. It is typically preceded by generation of dislocations and slip. Previous work concluded that a pinhole (i.e. a cavity from gas bubble in the melt) was the main cause of structure loss in an n-type Czochralski ingot. In the present study, seven industrial n-type Czochralski silicon ingots were investigated to assess whether pinholes frequently contribute to cause structure loss. Pinholes were found within 5 cm above the position where dislocations were generated in four out of the seven ingots. Slices were cut with the pinholes at one surface and etched with Sopori etchant. The pinholes did not appear to have affected the arrangements of etch pits in these samples and investigation of pinholes did not reveal the cause of structure loss. Furthermore, there were not significantly higher pinhole frequency before structure loss compared to ingots without structure loss among 4041 industrial ingots. Modeling of thermal stresses showed stress concentration around a pinhole, and it gives new insight into the level of stress the ingot can endure without generating dislocations and slip.

Keywords: B2. Semiconducting silicon, A2. Czochralski method, A1. Characterization, A1. Stresses, A1 Computer simulation, A1. Line defects.

1. Introduction

Continued cost reductions drive the fast growing market for solar electricity. The costs of monocrystalline silicon solar cells and modules are in part reduced by improving yield and reducing the production time of the Czochralski (Cz) process, which the monocrystalline silicon ingots are made from. Structure loss is one of the major industrial challenges for monocrystalline silicon production, which contribute to yield reduction and increased production time.

Structure loss means that the monocrystalline structure is lost as new grains start to form and the ingot becomes multicrystalline. Typically, the crystal grows for some time with increasing number of dislocations, particularly near the rim [1], before transitioning to multicrystalline

structure. Monocrystalline silicon ingots are also expected to be dislocation free, thus generation of dislocations impairs the ingot quality. The crystal also slips and dislocations are multiplied up to one crystal diameter into the already formed crystal [1]. If the structure loss is caused by a particle contacting the rim of the solidification front, new grains may nucleate directly on the particle and this may happen at the same time the crystal slips [2]. Formation of dislocations is observed visually by loss of nodes.

Nodes are vertical ridges that protrude from the cylindrical shape of the ingot. Ingots grown in the [100] direction have four nodes. According to Voronkov et al. [3], they form due to undercooling for nucleating new atomic planes during faceted growth in {111} planes in these areas. When dislocations are introduced in a (111) facet, new atomic planes can nucleate without high undercooling and the node is lost. This is observed as the ridge disappears and the rim of the crystal becomes fully cylindrical.

Lanterne et al. [1] investigated structure loss in an industrial ingot and traced dislocation arrays formed during slip to a pinhole at the solidification front at the time of node loss. A pinhole is a cavity in the crystal that originates from a gas bubble in the melt [4]. The size can be in the range of 50 μm - 2 mm [5], much larger than voids formed from agglomeration of vacancies. Bubbles may form at cavities in the crucible inner surface during melting [5], release of bubbles near the surface of the crucible as the inner layer is dissolved [6], and gas may be trapped under pieces of silicon and be incorporated as bubbles during melting [7]. Lanterne et al. [1, 2] concluded that crystallization of silicon around a pinhole was the main cause for structure loss in one of three n-type Cz ingot they investigated. However, pinholes are routinely observed as holes through wafers and do not always cause structure loss.

The present study investigates whether pinholes are a common cause of structure loss. This work characterizes seven industrial n-type Cz silicon ingots with structure loss. Pinholes are first found and characterized. Characterization of the structure losses is presented to show the transition from mono- to multicrystalline structure following loss of the nodes. The relation between pinholes and structure loss is discussed; by studying dislocation etch pits around pinholes and statistical analysis of data for industrial ingots. Thermal stresses are reported to facilitate dislocation generation [8, 9] and structure loss [10]. Thus, concentration of thermal stresses around a pinhole is modeled, and the contribution of stress concentration to structure loss is discussed.

2. Method

Seven industrial n-type Cz silicon ingots with structure loss were characterized. Ingots 1-3 had 8 inch diameter and ingots 4-7 had 6 inch diameter. The ingots had structure loss in the early body or crown. X-ray computed tomography (CT) was used to find pinholes in a disc typically between 5 cm above and below the loss of the first node. The discs were cut in four sectors to allow sufficient X-ray transmission, as shown schematically in Fig. 1. The X-ray CT used a voltage of 225 kV and a W target. Pinholes with diameters down to 0.2 mm could be observed. The position of pinholes inside the sectors were found and then 2 mm thick slices were cut in the direction along a

(001) or (010) plane in order to slice through the pinhole in one surface (see Fig. 4). For ingots without a pinhole above the first node loss, slices were cut between each sector.

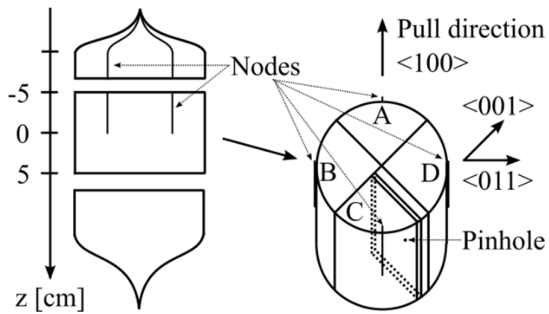


Fig. 1: Schematic view of the cutting of sectors A-D and a slice with a pinhole in one surface.

The slices were mechanically polished on both sides. Carrier density imaging (CDI) [11] and photoluminescence (PL) were attempted to visualize the slip pattern, but this was not clearly observed. Possibly, the samples did not extend high enough above the loss of the first node, as slip pattern is observed higher in the ingot investigated by Lanterne et al. [1] (Fig. 2). Additionally, the solidification front at the time of slip was not observed in the current samples. The samples were etched in Sopori etchant (HF:HNO₃:CH₃COOH 36:2:15) for 25 s and 5 s in HF:HNO₃ 1:9, after rinsing in RCA1 (H₂O:H₂O₂:NH₄OH 5:1:1) at 70°C and 5% HF. Resulting etch pits were studied by light microscopy. Lateral photovoltage scanning (LPS) was conducted on the samples with pinhole to visualize the solidification front at the time of first node loss, to be able to assess whether the pinholes were situated at the solidification front at this time or measure the height of the positions of the pinhole above the solidification front at time of first node loss.

In order to analyze the gas content in a pinhole, a small bar sample was made around a pinhole in sector 4B with a laser mark across the bar on either side of the pinhole. The analysis was performed by Zentrum für Glas- und Umweltanalytik GmbH, where the sample was loaded in a vacuum chamber and fractured at the laser mark so that the pinhole was opened and the gases released was measured by mass spectroscopy [12]. A sample was made for electron backscatter diffraction (EBSD) analysis where new grains appeared in ingot 2.

Statistical analysis was performed on data for 4041 industrial ingots. Ingots with and without structure loss were identified and combined with data on pinhole frequency. The ingots are cut in blocks before wafering and the pinhole data aggregates the number of wafers with pinholes for each block, and division by the total number of wafers from the block gives a frequency of pinholes as the percentage of wafers with pinholes in the block. The part of the ingot affected by structure loss is not wafered and the closest measurement of pinhole frequency is for the last block of ingots with structure loss. The analysis compares the frequency of pinholes in the last block of ingots with structure loss to a reference for ingots without structure loss. The data is collected for each block number as the frequency of pinholes decreases along the length of the ingot. For block 5 as an example, all ingots with structure loss and with block 5 as the last block is collected and the percentage of wafers with pinhole for block 5 is averaged among these ingots (see Fig. 5). Earlier blocks in these ingots are not included in the analysis of lower block numbers.

In order to estimate thermal stresses and stress concentration around a pinhole, a finite element method (FEM) model of an ingot during pulling was made in COMSOL Multiphysics® 5.3. First, the thermal field is modeled and this is coupled through thermal expansion to modeling of linear elastic material. The model is stationary. The geometry is shown in Fig. 2. The model is axisymmetric for a 6 inch diameter ($r = 76.2$ mm) crystal with height $h = 253$ mm up to the start of

the body. The top point is fixed while all other points and boundaries are free. The interface deflection is set to $H = 5.8$ mm. Different curvatures of the interface were tested (for the same deflection), but not found to have large impact on the results. The boundary for the solidification front was set to the melting temperature of silicon of 1687 K, and the other external boundaries were set to radiate to an ambient temperature of 1273 K. The crystal has a translational velocity of 1 mm/min upwards. A pinhole is modeled as a spherical cavity at the central axis, surrounded by a very fine mesh (6 μm mesh size along boundary).

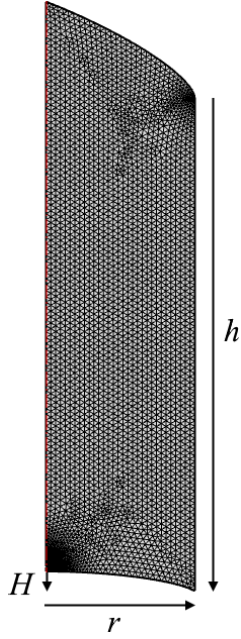


Fig. 2: Axisymmetric geometry with mesh and definition of parameters for FEM model.

The material properties used for modeling is as follows. The parameters are extrapolated to the melting point (1687 K) in the model. The thermal expansion coefficient (α) in K^{-1} is from Okada and Tokumaro [13] and Equation (1) is valid between 300 K and 1500 K:

$$\alpha(T) = 3.725 \cdot 10^{-6} \cdot (1 - e^{-5.88 \cdot 10^{-3} \cdot (T-124)}) + 5.548 \cdot 10^{-10} \cdot T \quad (1)$$

The thermal conductivity (k) in W/cm/K is in Equation (2) [14, 15].

$$k(T) = 10^{-1.2346 \cdot (\log(T) - 2.60206)} \quad (2)$$

The emissivity of the crystal was taken was taken from Timans [16] for their 78 Ωcm n-type sample between 553-941 K and from Jain et al. [17] for their 0.1 Ωcm n-type sample up to 1537 K. The

Young's modulus and Poisson's ratio are calculated by Reuss averaging of elastic coefficients C_{11} , C_{12} and C_{44} in MPa in Equations (3-5) [10, 18, 19], valid from 300 K to 1000 K.

$$C_{11} = 165640 \cdot e^{-9.4 \cdot 10^{-5} \cdot (T-298.15)} \quad (3)$$

$$C_{12} = 63940 \cdot e^{-9.8 \cdot 10^{-5} \cdot (T-298.15)} \quad (4)$$

$$C_{44} = 79510 \cdot e^{-8.3 \cdot 10^{-5} \cdot (T-298.15)} \quad (5)$$

3. Results and Discussion

Pinholes were identified inside the sectors by X-ray CT. Within 10 cm of the first node loss, a total of 10 pinholes were observed in the seven ingots investigated. All 10 identified pinholes have diameters of 0.5-0.7 mm. These sizes are within the range of pinholes detected in wafers [4, 5]. They have approximately equal height, width and depth and have approximately circular cross-sections in a vertical plane, as shown in Fig. 4.

The gas inside one pinhole was analyzed to be argon with trace of nitrogen. The pinhole was likely created from a bubble of the furnace atmosphere in the melt. The bubble may have formed during melting as the melt level was raised above a scratch or cavity in the crucible wall [5] or some gas may have been trapped under silicon pieces in the charge [7].

All investigated ingots had structure loss. The position of node losses relative to the start of body is given in Table 1. The transition to multicrystalline structure was studied by EBSD for ingot 2 (see Fig. 3). The sample was cut inwards from the rim of the ingot towards the center. New grains with high-angle grain boundaries grow from the rim, which was also observed by Lanterne et al. [1]. The new grains was observed to start forming 16 cm below the loss of the first node.

Ingot	Sector A	Sector B	Sector C	Sector D
1	-15 mm	-15 mm	-15 mm	-15 mm
2	-27 mm	-27 mm	-27 mm	-23 mm
3	332 mm	332 mm	332 mm	332 mm
4	253 mm	253 mm	253 mm	253 mm
5	12 mm	38 mm	14 mm	68 mm
6	64 mm	108 mm	69 mm	69 mm
7	18 mm	62 mm	21 mm	53 mm

Table 1: Height of node losses relative to start of body. Negative values indicate node loss in crown.

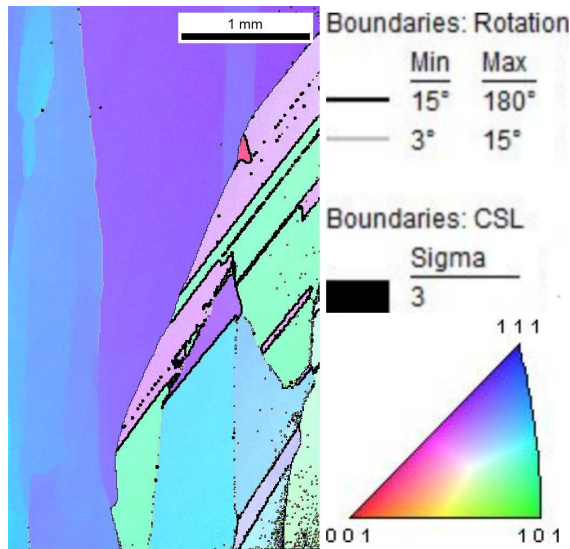


Fig. 3: Transition from monocrystalline to multicrystalline structure in ingot 2 revealed by EBSD (the crystal rim is towards the right).

Of the seven ingots with structure loss, pinholes were found up to 5 cm above the loss of the first node in four of the ingots. The position of pinholes above the solidification front at the loss of the first node is given in Table 2. None of the pinholes was situated at the solidification front at the time of the first node loss, while this was the position of the pinhole Lanterne et al. [1] suggested to contribute to cause structure loss. No trend was observed for the horizontal position of pinholes.

Pinhole	Height over solidification front at time of first node loss [mm]
1Da	29
3Aa	4
3Ba	11
5Da	7
7Ba	10

Table 2: Height of pinhole over solidification front at time of first node loss.

Slices were cut with pinholes in one surface and Sopori etched in order to study the arrangements of dislocations around the pinholes. Dislocation etch pits were recognized with typical sizes of 4-5 μm [1]. Lanterne et al. [1] observed two arrays of dislocations converging at the pinhole. The arrays are at 45° angle in slices cut along {001} planes and follow {111} slip planes in silicon. They concluded that dislocations were nucleated from the pinhole and that slip propagated from there. No such dislocation arrays were observed in any of the Sopori etched slices in this study, and the pinholes do not seem to have affected the arrangements of dislocations as exemplified in Fig. 4. This was also confirmed by dislocation density mapping with PVScan for slice 5Da. The slices were cut along (001) or (010) planes and contains two of the six slip directions in silicon. For dislocations to propagate throughout the ingot, slip must occur in directions contained in at least two {001} planes. Although possible, it is unlikely that none of the slices contained an active slip direction.

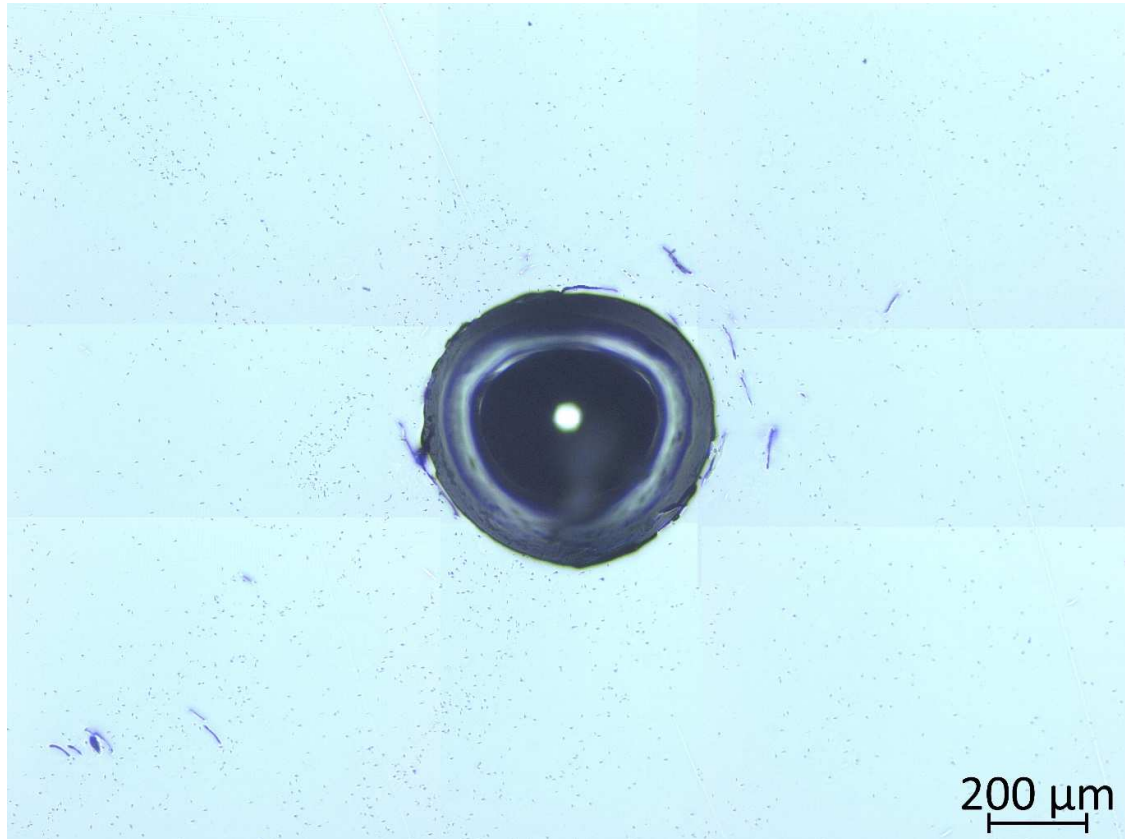


Fig. 4: Light micrograph around pinhole in Sopori etched slice 5Da.

In addition to investigating industrial sample ingots, statistical analysis of 4041 industrial ingots compares the frequency of pinholes before structure loss to a reference for ingots without structure loss in Fig. 5. For each block number, the two series compare the mean pinhole frequency for blocks which are the last block in an ingot with structure loss to the reference. A student t-test is performed for each block number to check if the two points are significantly different. The pinhole frequency before structure loss is not significantly higher than the reference without structure loss. If pinholes were a frequent cause of structure loss, a higher pinhole frequency would be expected to give a higher probability of structure loss, and thus that ingots with structure loss have a higher frequency of pinholes than ingots without structure loss.

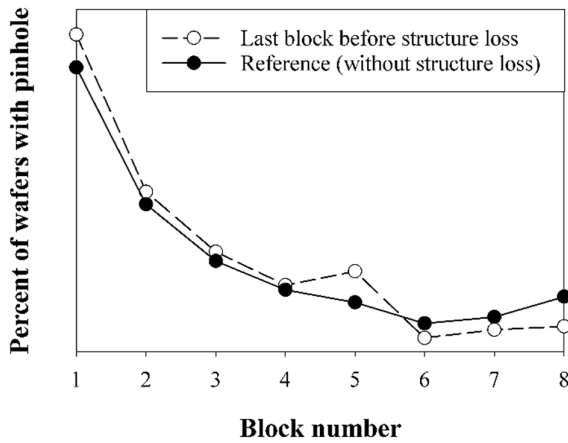


Fig. 5: Frequency of pinholes before structure loss compared to reference without structure loss.

The relatively high pinhole frequency in the first block and the gradually decreasing trend indicate that most bubbles in the melt are formed before growth of the ingots is started, by trapping of gas under pieces of silicon during melting [7] or formation at cavities in the crucible inner surface [5]. With a high initial concentration of bubbles in the melt, they will frequently be trapped at the solidification front. This reduces the concentration of bubbles in the melt and the frequency that bubbles are trapped at the solidification front is gradually reduced. The gradual release of bubbles near the surface of the crucible as the inner layer is dissolved [6] is not at a high enough rate to replenish the concentration of bubbles in the melt.

High thermal stresses are modeled in the crystal during growth [8-10, 18, 20-24]. The model in Fig. 6 provides a similar temperature profile as modeled by Muižnieks et al. [9], Smirnova et al. [23], Noghabi et al. [10] and Noghabi and M'Hamdi [24], although with a slightly higher radial temperature gradient, and the overall von Mises stress in Fig. 6b is in the upper range of previous models [9, 10, 18, 24]. The temperature profile and overall stress profile differ in the top and middle part of the crystal from models by Miyazaki et al. [18], Miyazaki and Okuyama [25], and Miyazaki and Kuroda [22], and consequently the modeled stress profile in this region.

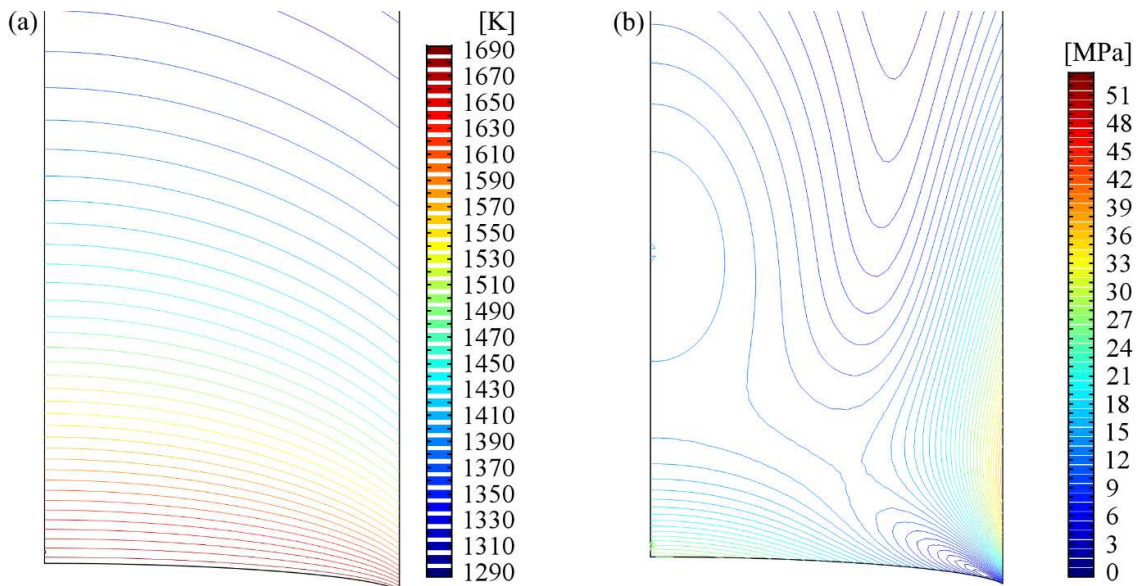


Fig. 6: Axisymmetric temperature profile (a) and von Mises stress (b) in lower part of ingot. For reference, the ingot radius is 76.2 mm.

Fig. 7 shows the model of a pinhole 2.5 mm above the solidification front at the center of the ingot. The thermal stresses are concentrated around the pinhole. The profile of the von Mises stress along the pinhole boundary from bottom to top of the pinhole is shown in Fig. 8a, normalized to the maximum von Mises stress. The stress concentration factor is calculated as the ratio of the maximum stress at the pinhole boundary (marked “max” in Fig. 7) to the stress level five pinhole diameters to the side of the pinhole (marked “avg” in Fig. 7), $\sigma_{\max}/\sigma_{\text{avg}}$. The maximum stress around the pinhole can be estimated for different radial positions of the pinhole by assuming the same stress concentration factor of 2.1 as in Fig. 7. At the same height as the pinhole in Fig. 7, a pinhole at half of the ingot radius would concentrate the stress to 40 MPa, and 63 MPa at the periphery of the ingot. At the maximum stress along the periphery of the ingot in Fig. 6b, the maximum stress around a pinhole is estimated to 79 MPa.

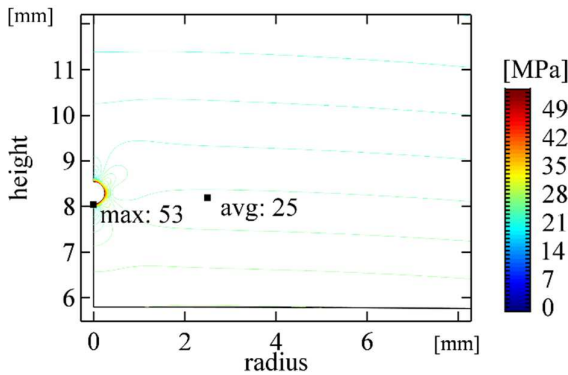


Fig. 7: Contour plot of von Mises stress around pinhole. The pinhole diameter is 0.5 mm and the contour spacing is 1 MPa. The left edge is the central axis and the bottom edge the solidification front.

The stress field around the pinhole and the stress concentration factor is relatively constant with changing pinhole diameter, at least for diameters between 50 μm and 2 mm. At a height of 2.5 mm above the solidification front, the stress concentration varies between 2.0 for a 0.1 mm diameter pinhole and 2.3 for a 2 mm diameter pinhole. The stress concentration factor is expected to be independent on pinhole size above nanometer scales [26].

The effect of vertical position of the pinhole, with diameter 0.5 mm, is shown in Fig. 8b. The stress concentration factor is around 2.1 from where the top of the pinhole is four pinhole radii above the solidification front and up to 13 mm above the solidification front. With further increasing height, the stress concentration factor gradually reduces to 1.7-1.8 from 24 mm above the solidification front, due to changing stress field around the pinhole. The model approaches a singularity as the pinhole closes when the top of the pinhole is two pinhole radii above the solidification front in Fig. 8b, as a sharp wedge with only one mesh node forms at the bottom of the pinhole. This region is left out of Fig. 8b.

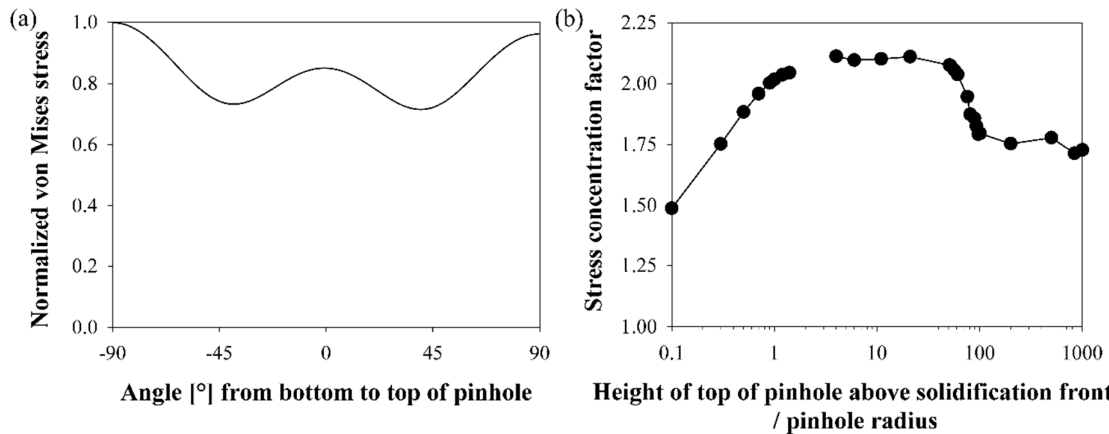


Fig. 8: Von Mises stress profile along pinhole boundary from bottom (-90°) to top (90°) of pinhole (a) and modeled stress concentration factor as function of vertical pinhole position for 0.5 mm diameter pinhole (b).

Jordan et al. [8] postulated that dislocations are first introduced by crystallographic glide caused by excessive thermal stress, above the critical resolved shear stress. The current estimate for the critical resolved shear stress is about 1 MPa at the melting point of silicon [9, 14]. Thermal stress in excess of the critical resolved shear stress is found in the lower part of crystals during growth in all models, except a model by Wijaranakula [21] for which he calculated an Arrhenius-type temperature dependence of the Young's modulus. Muižnieks et al. [9] reconciled the existence of dislocation-free crystals with stating that there is no direct relation between occurrence of dislocations and stress distribution. However, at points of high stress level, they suggested that dislocations might start to form due to a perturbation that provides a sufficient energy to break the ideal dislocation-free structure. They reasoned that the required perturbation energy is lower where the stress level is higher. Since pinholes are stress concentrators, they may potentially provide a region where the required perturbation energy is reduced and more perturbations would be able to start dislocation generation, and thus contribute to cause structure loss. However, it is not found that pinholes identified in four out of seven ingots contributed to cause structure loss in these ingots. On the other hand, the modeled stress concentration gives new insight into the level of stress the ingot can endure without causing slip and structure loss, as pinholes are routinely observed in wafers of successfully grown ingots. For 8 inch ingot with 20 mm interface deflection a maximum of ca. 80 MPa is modeled on the boundary of the pinhole. Von Ammon et al. [27] have experienced cracking of ingots when the highest calculated thermal stress increase beyond a critical value, in the range 80 – 100 MPa for their hot-zone.

Causes of structure loss suggested in literature are high stresses in the crystal, temperature fluctuations causing pulsation of the solidification rate with local and temporal remelting [23], particularly for a low temperature gradient at a node [28]. "W-shape" of the solidification front, particles incorporated in the solidification front and mechanical vibration of the crystal or crucible, or waves on the melt free surface [23] are also considered as causes for structure loss. Particles were not observed in any of the ingots and they did not have "W-shaped" solidification front. High stresses are also unlikely the cause of structure loss in the ingots with pinholes as dislocations were not generated where the stress concentrated to high values around pinholes. Temperature fluctuations remains as a possible cause of structure loss in the ingots and vibrations for ingots 3 and 7.

4. Conclusion

Seven industrial n-type Cz ingots with structure loss were investigated with X-ray CT and mass spectroscopy to identify and characterize pinholes. The transition to multicrystalline structure was studied with EBSD and found to start 16 cm below the loss of the first node in one ingot. Sopori etching was used to study arrangements of dislocation etch pits around pinholes. Statistical analysis between frequency of ingots and structure loss was performed for data on 4041 industrial ingots. A COMSOL Multiphysics® model was made to model thermal stresses and stress concentration around a pinhole. From these analyses, the main conclusions are as follows:

- Within 10 cm height of the seven ingots, 10 pinholes larger than 0.2 mm were observed with X-ray CT. The pinholes were approximately spherical with typical diameters 0.5-0.7 mm. The measurement on one of the pinholes indicated that the gas contained is Ar, which likely comes from the furnace atmosphere.
- Among four ingots with pinholes within 5 cm above the loss of the first node, the pinholes did not appear to have affected the arrangement of dislocation etch pits and there were no indication that pinholes caused the structure loss.
- The pinhole frequency before structure loss is not significantly higher than the reference for ingots without structure loss.
- Modeling of thermal stresses and stress concentration around a pinhole in the center of the ingot gives a stress concentration factor of around 2.1 when the pinhole is fully inside the crystal and up to a height of 13 mm above the solidification front.

Accordingly, pinholes do not appear to be a common cause of structure loss, and the stress does not appear to be concentrated to high enough values to generate dislocations and cause structure loss.

5. Acknowledgements

This work was performed within the Research Centre for Sustainable Solar Cell Technology (FME SuSolTech, project number 257639), co-sponsored by the Norwegian Research Council and research and industry partners. The funding source has no involvement in the preparation or submission of the article. NorSun AS is gratefully acknowledged for providing ingots investigated in this work and industrial data. The works of Michael Schrepf at Zentrum für Glas- und Umweltanalytik GmbH with testing samples and analyzing the gas content in pinholes, Rune Søndena at Institute for Energy Technology with PL measurements, Gaute Stokkan at SINTEF Industry with PVScan measurements and Siw Anita Hansen with CDI measurements at Department of Materials Science and Engineering, NTNU, are greatly appreciated.

6. References

- [1] A. Lanterne, G. Gaspar, Y. Hu, E. Øvrelid and M. Di Sabatino: Characterization of the loss of the dislocation-free growth during Czochralski silicon pulling, *J. Cryst. Growth* Vol 458 (2017), pp. 120-128. <https://doi.org/10.1016/j.jcrysgro.2016.10.077>.
- [2] A. Lanterne, G. Gaspar, Y. Hu, E. Øvrelid and M. Di Sabatino: Investigation of different cases of dislocation generation during industrial Cz silicon pulling, *Phys. Status Solidi C*, Vol 13 (2016), No. 10-12, pp. 827-832. <https://doi.org/10.1002/pssc.201600063>.
- [3] V. V. Voronkov, B. Dai and M S. Kulkarni: Fundamentals and Engineering of the Czochralski Growth of Semiconductor Silicon Crystals, in *Comprehensive Semiconductor Science and*

- Technology, P. Bhattacharya, R. Fornari, H. Kamimura (eds), Elsevier B. V., 2011, Vol 3, ISBN 978-0-444-53143-7, pp. 87-94. <https://doi.org/10.1016/B978-0-44-453153-7.00089-4>.
- [4] J. Paloheimo: Properties of Silicon Crystals, in Handbook of Silicon Based MEMS Materials and Technologies (1st ed.), V. Lindroos, M. Tilli, A. Lehto, T. Motooka (eds), William Andrew Publishing, 2010, ISBN 978-0-8155-1594-4, p. 50. <https://doi.org/10.1016/B978-0-8155-1594-4.00055-3>.
- [5] T. Minami, S. Maeda, M. Higasa and K. Kashima: In-situ observation of bubble formation at silicon melt-silica glass interface, J. Cryst. Growth Vol 318 (2011), pp. 196-199. <https://doi.org/10.1016/j.jcrysgro.2010.10.075>.
- [6] X. Huang, H. Kishi, S. Oishi, H. Watanabe, K. Sanpei, S. Sakai and K. Hoshikawa: Expansion Behavior of Bubbles in Silica Glass Concerning Czochralski (Cz) Si Growth, Jpn. J. Appl. Phys. Vol 38 (1999), No. 4A, pp. L353-L355. <https://doi.org/10.1143/JJAP.38.L353>.
- [7] H. W. Korb, R. Phillips: Reduction of Air Pockets in Silicon Crystals by Avoiding the Introduction of Nearly-insoluble Gases into the Melt (2009), US2009/0120353 A1, United States, Google Patents.
- [8] A. S. Jordan, R. Caruso, A. R. Von Neida and J. W. Nielsen: A comparative study of thermal stress induced dislocation generation in pulled GaAs, InP, and Si crystals, J. Appl. Phys. Vol 52 (1981) pp. 3331-3336. <https://doi.org/10.1063/1.329154>.
- [9] A. Muižnieks, G. Raming, A. Mühlbauer, J. Virbulis, B. Hanna and W.v. Ammon: Stress-induced dislocation generation in large FZ- and CZ-silicon single crystals – numerical model and qualitative considerations, J. Cryst. Growth, Vol 230 (2001), pp. 305-313. [https://doi.org/10.1016/S0022-0248\(01\)01322-7](https://doi.org/10.1016/S0022-0248(01)01322-7).
- [10] O. A. Noghabi, M. M'Hamdi and M. Jomâa: Impact of diameter fluctuations on thermal stresses during Czochralski silicon growth, J. Cryst. Growth Vol 362 (2013), pp. 312-318. <https://doi.org/10.1016/j.jcrysgro.2011.11.025>.
- [11] S. A. Hansen: Structure Loss in Monocrystalline Silicon Ingots for Solar Cells, Department of Materials Science and Engineering, Norwegian University of Science and Technology, 2017.
- [12] Zentrum für Glas- und Umweltanalytik GmbH, <http://www.zgu.de/english/thermal-analyses-bubble-analysis.php> (August 21, 2018).
- [13] Y. Okada and Y. Tokumaru: Precise determination of lattice parameter and thermal expansion coefficient of silicon between 300 and 1500 K, J. Appl. Phys Vol 56 (1984), No. 2, pp. 314-320. <https://doi.org/10.1063/1.333965>.
- [14] A. S. Jordan, A. R. Von Neida and R. Caruso: The Theoretical and Experimental Fundamentals of Decreasing Dislocations in melt Grown GaAs and InP, J. Cryst. Growth Vol 79 (1986), pp. 243-262. [https://doi.org/10.1016/0022-0248\(86\)90445-8](https://doi.org/10.1016/0022-0248(86)90445-8).
- [15] M. Neuberger: Group IV Semiconducting Materials, Handbook of Electronic Materials, Vol V,IFI/Plenum, New York, 1971, ISBN 978-1-4684-7917-1.
- [16] P. J. Timans: Emissivity of silicon at elevated temperatures, J. Appl. Phys. Vol 74 (1993), pp. 6353-6364. <https://doi.org/10.1063/1.355159>.
- [17] S. C. Jain, S. K. Agarwal, W. N. Borle and S. Tata: Total emissivity of silicon at high temperatures, J. Phys. D: Appl. Phys. Vol 4 (1971), pp. 1207-1209. <https://doi.org/10.1088/0022-3727/4/8/323>.

- [18] N. Miyazaki, H. Uchida and T. Munakata: Thermal stress analysis of silicon bulk single crystal during Czochralski growth, *J. Cryst. Growth* Vol 125 (1992), pp. 102-111. [https://doi.org/10.1016/0022-0248\(92\)90325-D](https://doi.org/10.1016/0022-0248(92)90325-D).
- [19] INSPEC: Properties of Silicon, EMIS Datareviews Series, No. 4 (1988), ISBN 0852964757, p. 14.
- [20] D. E. Bornside, T. A. Kinney and R. A. Brown: Minimization of thermoelastic stresses in Czochralski grown silicon: application of the integrated system model, *J. Cryst. Growth* Vol 108 (1991), pp. 779-805. [https://doi.org/10.1016/0022-0248\(91\)90260-C](https://doi.org/10.1016/0022-0248(91)90260-C).
- [21] W. Wijaranakula: A Real-Time Simulation of Point Defect Reactions Near the Solid and Melt Interface of a 200 mm Diameter Czochralski Silicon Crystal, *J. Electrochem Soc.* Vol 140 (1993) No. 11, pp. 3306-3316. <https://doi.org/10.1149/1.2221028>.
- [22] N. Miyazaki and Y. Kuroda: Dislocation Density Simulations for Bulk Single Crystal Growth Process, *Met. Mater.* Vol 4 (1998) No. 4, pp. 883-890. <https://doi.org/10.1007/BF03026417>.
- [23] O. V. Smirnova, N. V. Durnev, K. E. Shandrakova, E. L. Mizitov and V. D. Soklakov: Optimization of furnace design and growth parameters for Si Cz growth, using numerical simulation, *J. Cryst. Growth* Vol 310 (2008), pp. 2185-2191. <https://doi.org/10.1016/j.jcrysgro.2007.11.204>.
- [24] O. A. Noghabi and M. M'Hamdi: Anisotropic study of thermal stresses induced by diameter fluctuation during Czochralski silicon single crystal growth, *J. Cryst. Growth* Vol 400 (2014), pp. 1-6. <https://doi.org/10.1016/j.jcrysgro.2014.04.027>.
- [25] N. Miyazaki and S. Okuyama: Development of finite element computer program for dislocation density analysis of bulk semiconductor single crystals during Czochralski growth, *J. Cryst. Growth* Vol 183 (1998), pp. 81-88. [https://doi.org/10.1016/S0022-0248\(97\)00388-6](https://doi.org/10.1016/S0022-0248(97)00388-6).
- [26] P. Sharma and S. Ganti: Size-Dependent Eshelby's Tensor for Embedded Nano-Inclusions Incorporating Surface/Interface Energies, *J. Appl. Mech.* Vol 71 (2004), pp. 663-671. <https://doi.org/10.1115/1.1781177>.
- [27] W. von Ammon, E. Dornberger and P. O. Hansson: Bulk properties of very large diameter silicon single crystals, *J. Cryst. Growth* Vol 198/199 (1999), pp. 390-398. [https://doi.org/10.1016/S0022-0248\(98\)01140-3](https://doi.org/10.1016/S0022-0248(98)01140-3).
- [28] L. Stockmeier: Heavily n-type doped silicon and the dislocation formation during its growth by the Czochralski method, *Der Technischen Fakultät, Friedrich-Alexander-Universität Erlangen-Nürnberg*, 2017, p. 125.